

Effect of the distance between focusing lens and target surface on quantitative analysis of Mn element in aluminum alloys by using filament-induced breakdown spectroscopy

Xue-Tong Lu(陆雪童), Shang-Yong Zhao(赵上勇), Xun Gao(高勋), Kai-Min Guo(郭凯敏), and Jing-Quan Lin(林景全)

Citation: Chin. Phys. B, 2020, 29 (**12**): 124209. DOI: 10.1088/1674-1056/abb3ef
Journal homepage: http://cpb.iphy.ac.cn; http://iopscience.iop.org/cpb

What follows is a list of articles you may be interested in

High efficiency sub-nanosecond electro-optical *Q*-switched laser operating at kilohertz repetition frequency

Xin Zhao(赵鑫), Zheng Song(宋政), Yuan-Ji Li(李渊骥), Jin-Xia Feng(冯晋霞), Kuan-Shou Zhang(张宽收)
Chin. Phys. B, 2020, 29 (**8**): 084205. DOI: 10.1088/1674-1056/ab8ac4

Gain-induced large optical torque in optical twist settings

Genyan Li(李艮艳), Xiao Li(李肖), Lei Zhang(张磊), Jun Chen(陈君)
Chin. Phys. B, 2020, 29 (**8**): 084201. DOI: 10.1088/1674-1056/ab9616

Optical nonreciprocity in a piezo-optomechanical system

Yu-Ming Xiao(肖玉铭), Jun-Hao Liu(刘军浩), Qin Wu(吴琴), Ya-Fei Yu(於亚飞), Zhi-Ming Zhang(张智明)
Chin. Phys. B, 2020, 29 (**7**): 074204. DOI: 10.1088/1674-1056/ab8abf

A low-noise, high-SNR balanced homodyne detector for the bright squeezed state measurement in 1-100 kHz range

Jin-Rong Wang(王锦荣), Qing-Wei Wang(王庆伟), Long Tian(田龙), Jing Su(苏静), Yao-Hui Zheng(郑耀辉)
Chin. Phys. B, 2020, 29 (**3**): 034205. DOI: 10.1088/1674-1056/ab683b

Optical enhanced interferometry with two-mode squeezed twin-Fock states and parity detection

Li-Li Hou(侯丽丽), Shuai Wang(王帅), Xue-Fen Xu(许雪芬)
Chin. Phys. B, 2020, 29 (**3**): 034203. DOI: 10.1088/1674-1056/ab6837

Effect of the distance between focusing lens and target surface on quantitative analysis of Mn element in aluminum alloys by using filament-induced breakdown spectroscopy*

Xue-Tong Lu(陆雪童)[1], Shang-Yong Zhao(赵上勇)[1], Xun Gao(高勋)[1,†], Kai-Min Guo(郭凯敏)[2,‡], and Jing-Quan Lin(林景全)[1]

[1] School of Science, Changchun University of Science and Technology, Changchun 130012, China
[2] School of Physical Science and Technology, Baotou Teachers' College, Baotou 014030, China

(Received 17 June 2020; revised manuscript received 13 July 2020; accepted manuscript online 1 September 2020)

Ultrafast laser filament-induced breakdown spectroscopy (FIBS) is a potential technique for quantitative analysis of trace elements. In this work, we investigate the effect of the distance between focusing lens and target surface on the FIBS quantitative analysis of Mn element in aluminum alloys, and several major parameters are calculated such as the linear correlation coefficient (R^2), limits of detection (LOD), relative standard deviation (RSD), and root-mean-square error of cross-validations (RMSECV). The results show that the quantitative analysis parameter values before and after filament position are different. The optimal value can be obtained at the filament region, the average values of total 23 positions of R^2, LOD, RSD, and RMAECV were 99.45%, 1.41 mg/kg, 7.12%, and 0.56%, respectively. Besides, the spatial distributions of quantitative analysis parameter values in filament region are noticeable, and this is essentially due to intensity clamping effect in a filament.

Keywords: filament-induced breakdown spectroscopy, limits of detection, relative standard deviation, root-mean-square error of cross-validations

PACS: 42.62.Fi, 52.38.Hb **DOI:** 10.1088/1674-1056/abb3ef

1. Introduction

Laser-induced breakdown spectroscopy (LIBS) as a rapid, *in situ*, real-time, noninvasive, and multi-elements analytical method has been attractively employed in a wide range of applications, such as aerosol, biomedical, pharmaceutical materials, environment, and cultural heritage objects analysis.[1,2] Typically, LIBS is performed using nanosecond laser pulse. The nanosecond laser has a long pulse width. The front edge of the pulse laser generates plasma, and the interaction between the trailing edge and the plasma is relatively complicated. Due to the effects of spectral self-absorption, matrix effects and plasma shielding, problems such as plasma and energy jitter will be caused.[3,4] And ns-LIBS are usually tightly focused transmissions. The different distances between focusing lens and target surface make the light spot have different sizes on target surface, causing changes in spectral intensity and spectral characteristics, which affects the detection accuracy, signal stability, and repeatability of the experiment. Therefore, LIBS has a strong dependence on the distance between focusing lens and target surface.[5,6]

Compared with ns-LIBS, femtosecond laser-induced breakdown spectroscopy (fs-LIBS) has the advantages with accurate ablation threshold, small thermal effect, high ablation efficiency, and little damage, which can improve the stability of LIBS technology.[7,8] The combination of femtosecond filament ablation and emission spectroscopy is a potential analytical tool for trace element detection. Filament of femtosecond pulse lasers, resulting from a dynamic interplay between optical Kerr self-focusing and plasma de-focusing processes, the power density varies from 10^{13} W/cm^2 to 10^{14} W/cm^2 because of the intensity clamping effect in filament. The filament can propagate over very large distances without suffering from optical geometry focusing effect and diffraction effect.[9,10] Filament-induced breakdown spectroscopy (FIBS) can cause a more uniform effect on the sample surface, which can eliminate the effect of the distance between focusing lens and sample surface on the laser-induced breakdown spectral intensity and spectral characteristics. In hazardous environments, telescope systems or fiber optic transmission can be used to conduct long-distance contactless analysis of toxic and hazardous substances, including nuclear radiation environments, explosive analysis, isotope analysis, environmental analysis, and soil contamination analysis.[11–16]

Ghebregziabher *et al.*[17] reported the characteristics of copper plasma induced by the filament and studied the spec-

*Project supported by the National Natural Science Foundation of China (Grant No. 61575030), the Natural Science Foundation of Jilin Province, China (Grant Nos. 20180101283JC and 20200301042RQ), and the Fund from the Department of Education of Jilin Province, China (Grant No. JJKH20190539KJ).

†Corresponding author. E-mail: lasercust@163.com
‡Corresponding author. E-mail: guokm@163.com

© 2020 Chinese Physical Society and IOP Publishing Ltd

tral intensity, plasma temperature, electron density, and signal-to-background ratios (SBR) trends at different locations of the filament. Harilal *et al.*[10] studied plasma temperature clamping by ablating brass and obtained the spatial evolution of radiation intensity and electron density propagating along the filament channel. Zhao *et al.*[18] investigated the spatial evolution of soil plasma radiation intensity, plasma temperature, and electron density induced by femtosecond laser filament, and calculated the LOD and R^2 at different positions of the filament. Yao[19] studied the effect of pulse energy on the plasma characteristics of filament ablation soil, and also studied the ablation of soil by combining filament and energy bank. It is well known that the properties of laser-induced plasma strongly depend on the laser irradiation conditions, such as laser energy, focus position, *etc*. Therefore, it is important to better understand the effect of the distance between focusing lens to target surface on the detection of FIBS trace elements. As far as we know, there is relatively little research on the effect of the distance between focusing lens and target surface on the quantitative analysis of trace elements in aluminum alloys by using FIBS. We hope that our research can provide a reference for FIBS in trace element detection and alloys material analysis technology.

In this paper, we change the distance between focusing lens and target surface, the aluminum alloys are ablated by filament and the Mn element is quantitatively analyzed. Several major parameters such as the linear correlation coefficient (R^2), limits of detection (LOD), relative standard deviation (RSD), and root-mean-square error of cross-validations (RMSECV) are calculated. The three areas of filament, before and after filament ablation are compared and the influence of focus position ablation on quantitative analysis of parameters is also investigated.

2. Experiments and methods

Figure 1 is a schematic diagram of the experimental setup. A laser (Libra-Usp-He, Coherent, USA) was used to produce the filament with the central wavelength of 800 nm, repetition rate of 1 kHz, and pulse width of 50 fs. A K9 glass lens lens 1 (focal length $f = 1000$ mm, mounted on a one-dimensional (1D) translation stage) is used to focus the femtosecond laser beam with the energy of 2.6 mJ. A fused silica lens lens 2 ($f = 75$ mm) was used to collect the plasma emission spectral signal, and coupled to a grating spectrometer (Spectra Pro500i, PI Acton, the grating is 1200 grooves/mm) equipped with an ICCD (PI MAXII, Princeton Instruments, 1024×256 pixel) with the entrance slit of 30 μm, spectral response range 200 nm–900 nm and resolution of 0.05 nm at 500-nm blaze wavelength. ICCD is triggered by a femtosecond laser. In order to avoid excessive ablation of the sample, the aluminum alloy sample is positioned on a three-dimensional (3D) translation stage (PI) setup. To ensure the signal stability over each experiment, plasma spectrum is averaged over 50 shots. Five repeating spectra at each point of the sample are recorded. The experiment condition is standard atmospheric pressure, room temperature of 22 °C, and relative humidity of 25%.

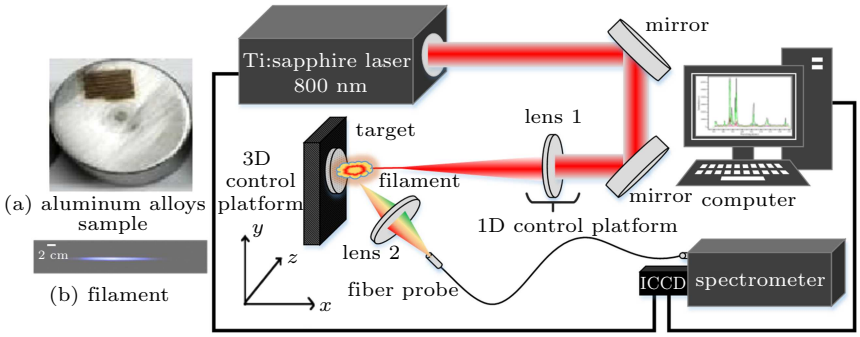


Fig. 1. The schematic diagram of experimental setup.

In our experiments, the six aluminum alloy samples of the LD7.8 series with diameter 6 cm and thickness 3 cm are selected, the concentration of the Mn element are shown in Table 1.

Table 1. The concentrations of Mn element in aluminum alloy samples (in unit wt%).

Element	E311	E312a	E313	E314	E315	E316
Mn	0.095	0.119	0.239	0.184	0.287	0.054
Mg	0.428	1.37	0.897	1.80	2.26	0.074

3. Results and discussion

Figure 2 shows the filament-induced aluminum alloy plasma spectroscopy at distances 970 mm between focusing lens and target surface. In our experiment, the detection spectrum wavelength range is 382 nm–423 nm, and four lines of Al I 383.83 nm, Al I 394.4 nm, AI 396.15 nm, and Mn I 403.31 nm are detected. The detection effect of FIBS on trace elements is studied, the matrix element Al is not considered. Compared with the Mg element, Mn element is relatively less

disturbed and the line intensity is higher. Therefore, we selected the Mn element for quantitative analysis in the experiment.

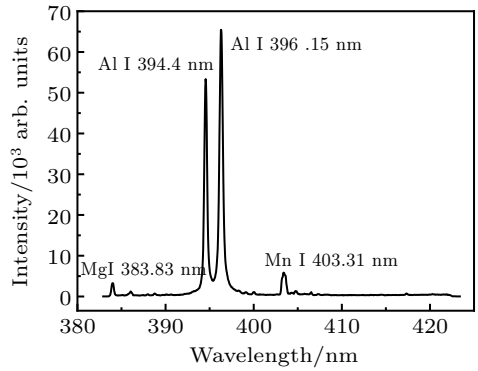


Fig. 2. Filament-induced aluminum alloy plasma spectroscopy for sample type E313, delay time 980 ns.

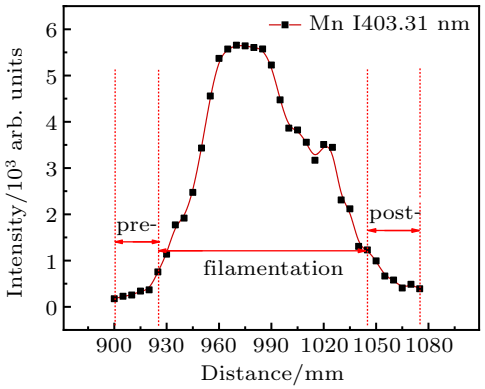


Fig. 3. Spatial distribution of Mn I 403.31-nm spectral intensity for sample type E313, delay time 980 ns.

Figure 3 shows the spatially-resolved Mn I 403.31-nm spectral intensity. The filament length is determined by fluorescence spectroscopy. The measurement error of the spectral line intensity is 14.52%. The possible causes of the error include the following: the uneven distribution of manganese in the sample, the fluctuation of the laser output energy, and the change in the ionization degree in the filament causes the spectral signal to fluctuate greatly. Increasing the detection position and acquisition time can reduce the measurement error.[20] We can see a high spectral line intensity in the range of 930 mm–1040 mm, and the distance about 110 mm. The spectral intensity of Mn I 403.31 nm first increases and then decreases with the distance from the focusing lens to the sample surface. There are two spectral intensity peaks at the distances of 970 mm and 1020 mm between focusing lens and target surface. Due to the optical Kerr self-focusing effect, the first focal point (970 mm) is shorter than the geometric focal point, and a strong plasma emission is generated at this position.[21] Because Kerr self-focusing and plasma defocusing will produce plasma filaments. Part of the energy of the laser pulse is released into the "energy reservoir" around the filament, and the energy bank continuously compensates the energy loss during the ablation of the aluminum alloys and plays a role in assisting the ablation.[22–24] Therefore, the ablation efficiency of filament depends both on clamped filament intensity and the rest of the laser energy in the energy reservoir of filament, which means that there exists non-uniform distribution for the plasma emission spectral intensity along the filament channel propagation. The refocusing position at 1020 mm, which is due to the effect of spectral broadening, to promoting geometric focusing effect of filaments and ionization effect. Because the ionization of air consumes part of the laser energy, the emission intensity at the refocusing position (1020 mm) is lower than the emission intensity at the first focusing position.[25]

When the initial power $P_{\rm in}$ of the femtosecond laser pulse is higher than the self-focusing critical power $P_{\rm cr}$, filaments will be generated. We used the moving focus model or spatial dynamic compensation model to describe the dynamic process of femtosecond pulsed laser self-focusing. According to the semi-empirical Marburger formula, the self-focusing collapse position $L_{\rm c}$ (where the beam radius is the smallest along the propagation direction) is[21,26]

$$L_{\rm c}=\frac{0.367kw_0^2}{\left\{\left[(P_{\rm in}/P_{\rm cr})^{1/2}-0.852\right]^2-0.0219\right\}^{1/2}}. \tag{1}$$

For a Gaussian beam, the critical power for self-focusing is $P_{\rm cr}=3.77\lambda_0^2/8\pi n_0 n_2$, $P_{\rm cr}=3$ GW, k is the wavenumber of the laser, and the beam radius w_0 is 3.8 mm. The peak power $P_{\rm in}$ of the incident pulse with a pulse width of 50 fs is 5.2×10^{10} W. The position d where the filament starts to form is[27]

$$d=\frac{f\times L_{\rm c}}{f+L_{\rm c}}, \tag{2}$$

where f is the geometric focal length of the lens, the calculated result is $d=926$ mm.

We know that the filament processes result in from a dynamic interplay between optical Kerr self-focusing and plasma de-focusing processes. Before and after filament, the power intensity is different. According to the trend of the intensity of the spectral line, we have judged that the filament ends at approximately 1040 mm. Hence, the filament length is about 114 mm, which is similar to the filament length measured by the fluorescence spectroscopy method. For the convenience of the above discussion, we choose 930 mm as the start position of filament. We mainly studied three intervals ranges: (i) the pre-filament area (900 mm–925 mm); (ii) the filament area (930 mm–1040 mm); (iii) the post-filament area (1045 mm–1075 mm). A filament is the propagation zone where there exists intensity clamping. The zones before and after the plasma

zone, where the intensity is still relatively high but not sufficient to generate a plasma, could be conveniently called pre- and post-filament zones.[9]

Figure 4 shows the spectral stability with the accumulation of 100 pulses of the three positions at 920 mm, 985 mm, and 1050 mm. We can see that the stability of the filament region is better than the pre- and post-filament areas, and the pre-filament is better than the post-filament. This phenomenon is because the stability of laser power affects the stability of radiation plasma, and the stability of plasma affects the stability of the spectrum.[28] Figure 5 shows the slope of the calibration curve at 920 mm, 1025 mm, and 1050 mm. We can see that the slope of the calibration curve at the filament center is higher than that at the pre- and post-filaments.

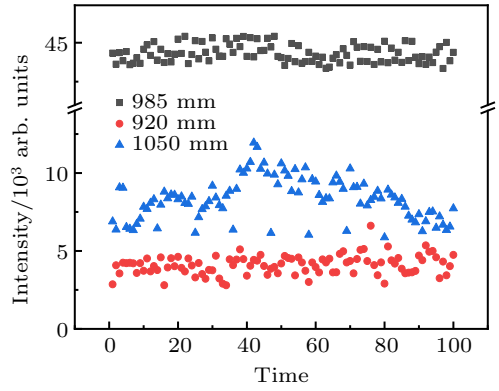


Fig. 4. Spectral stability at three positions along the filament (pre-filament at 920 mm, filament at 985 mm, and post-filament at 1050 mm, respectively).

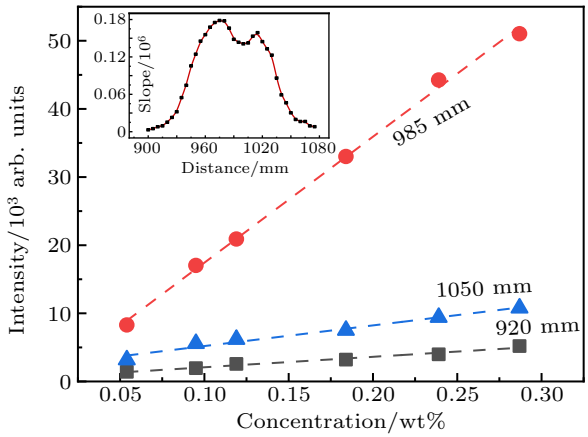


Fig. 5. Calibration curves of Mn element at different positions: pre-filament at 920 mm, filament at 985 mm, and post-filament at 1050 mm, respectively.

To estimate the spatially distribution law of FIBS for quantitative analysis parameters of Mn element in aluminum alloys, several major values such as R^2, LOD, RSD, and RMSECV are used as evaluation parameters. Their expressions are given below:[29–31]

$$R^2 = \frac{\left[\sum_{i=1}^{n}(x_i-\bar{x})(y_i-\bar{y})\right]^2}{\sum_{i=1}^{n}(x_i-\bar{x})^2 \times \sum_{i=1}^{n}(y_i-\bar{y})^2}, \tag{3}$$

where x_i and y_i are the concentration and spectral radiation intensity of sample i, respectively; x and y are the average values of x_i and y_i in n samples, respectively.

$$\mathrm{LOD} = 3\frac{\delta}{\varepsilon}, \tag{4}$$

where δ is the standard deviation of the spectral radiation background signal, and ε is the slope of the spectral radiation intensity calibration curve.

$$\mathrm{RSD} = \frac{[\sum (X_i - M)^2/(n-1)]^{1/2}}{M}, \tag{5}$$

where X_i is the i-th measured spectral radiant intensity, M is the average of the intensity of n measurements.

$$\mathrm{RMSECV} = \sqrt{\frac{\sum_i^n \left(C_i - C_i^{\mathrm{ref}}\right)^2}{n}}, \tag{6}$$

where C_i is the predicted concentration, C_i^{ref} is the reference concentration, n is the number of calibration samples.

The spatial distribution of quantitative analysis parameters are shown in Fig. 6. We can see that the filament region (930 mm–1040 mm) of R^2 is higher, and the LOD, RSD, and RMSECV are lower. The pre- (900 mm–925 mm) and post-filament (1045 mm–1075 mm) of R^2 are smaller, and the LOD, RSD, and RMSECV are higher. Table 2 shows the average value of the quantitative analysis parameters in the filament region (930 mm–1040 mm) and the two areas of pre- and post-filaments (900 mm–925 mm and 1045 mm–1075 mm). In the filament area, the average value of the correlation coefficient of the calibration curve R^2 is 99.53%, the average value of LOD is 1.41 mg/kg, the average value of the RSD is 7.12%, and the average value of RMSECV is 0.56%. Compared with the areas before and after filaments, the filaments region has better detection sensitivity, reproducibility, detection accuracy, and lower prediction concentration error.[31] The reason is that during the propagation of filaments, the energy in the energy reservoir is continuously added to the plasma filaments, to supplement the incident light energy consumed by nonlinear processes such as multi-photon ionization and diffraction of the beam itself. When Kerr self-focusing and plasma defocusing reach a dynamic equilibrium, due to the intensity clamping effect,[10] the laser pulse has a stable spatial distribution with an improved stability of laser transmission in the filament area, further improves the sensitivity and accuracy of quantitative analysis. Thus, in the filament area, the quantitative analysis parameters are relatively stable and superior to pre- and post-filament areas. Starting from self-focusing, before the pulse collapses, there was already some weak ionizations in the pulse contraction area.[9] The power density of post-filament is lower than the self-focusing critical power, and the

diffraction and dispersion effects are stronger than the self-focusing effect. The laser beam is in a divergent state,[32] and its spectral stability is lower than pre-filament area. Therefore, the spatial distribution of the quantitative analysis parameters is not uniform. In the post-filament area, the main physics mechanism is thermal ablation resulting from spectral broadening and optical geometry focusing effect.

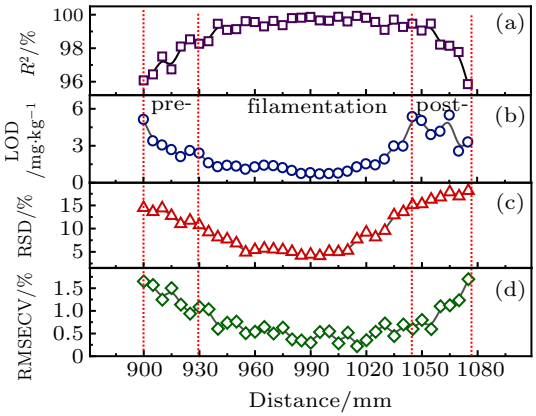


Fig. 6. The spatial distribution of FIBS quantitative analysis parameters: (a) R^2, (b) LOD, (c) RSD, and (d) RMSECV.

Table 2. The average value of the FIBS quantitative analysis parameters.

Distance/mm	LOD/(mg/kg)	RSD/%	RMSECV/%	R^2/%
900–925	3.16	13	1.34	97.22
930–1040	1.41	7.12	0.56	99. 45
1045–1075	4.26	16.37	1.02	98.28

4. Conclusions

In this paper, FIBS technique is used to study the variation of quantitative analysis parameters of Mn in aluminum alloys with the distance between focusing lens and target surface. Comparing with the pre-filament area, filament area, and post-filament area, we found that the optimal value can be obtained at the filament region, the average values of total 23 positions of R^2, LOD, RSD, and RMAECV are 99.45%, 1.41mg/kg, 7.12%, and 0.56%, respectively. Because of the intensity clamping effect in filament, the filament can propagate over very large distances without suffering from optical geometry focusing effect and diffraction effect. The quantitative analysis parameters are better than those of the pre- and post-filament areas, this indicates that different distances of the sample surface to the focusing lens have an impact on the detection accuracy and spectral stability ability. Therefore, FIBS is a useful approach to quantitative analysis of trace elements, and can provide great reference value for applications of FIBS.

References

[1] Xiu J S, Zhong S L, Hou H M, Lu Y and Zheng R E 2014 *Appl. Spectrosc.* **68** 1039
[2] Awan M A, Ahmed S H, Aslam M R, Qazi I A and Baig M A 2013 *Arab. J. Sci. Eng.* **38** 1655
[3] Anzano J M, Villoria M A, Ruíz-Medina A and Lasheras R J 2006 *Analytica Chimica Acta* **575** 230
[4] Aragón C, Bengoechea J and Aguilera J A 2001 *Spectrochim. Acta B: At. Spectrosc.* **56** 619
[5] Liu Y H, Chen M, Liu X D, Cui Q Q and Zhao M W 2013 *Acta Phys. Sin.* **62** 025203 (in Chinese)
[6] Wang Y, Chen A M, Wang Q Y, Sui L Z, Ke D, Cao S, Li S Y, Jiang Y F and Jin M X 2018 *Phys. Plasmas* **25** 033302
[7] Drogoff B L, Vidal F, Kaenel Y and Chaker M 2001 *J. Appl. Phys.* **89** 8247
[8] Zhao Q C, Dai Y T, Li T, Liu B, Yang H M and Yin G L 2014 *Opt. Lett.* **39** 1905
[9] Chin S L 2010 *Femtosecond Laser Filamentation* (New York: Springer)
[10] Harilal S S, Yeak J and Phillips M C 2015 *Opt. Express* **23** 27113
[11] Shaik A K and Soma V R 2019 *OSA Continuum* **2** 554
[12] Harilal S S, Diwakar P K and Lahaye N L 2015 *Spectrochim. Acta B: At. Spectrosc.* **111** 1
[13] Hartig K C, Ghebregziabher I and Jovanovic I 2017 *Sci. Rep.* **7** 43852
[14] Kalam S A, Ajmathulla and Rao S V 2018 *Opt. Lett.* **43** 3465
[15] Li W T, Zhu Y N, Li X, Hao Z Q, Guo L B, Li X Y, Zeng X Y and Lu Y F 2018 *J. Anal. At. Spectrom.* **33** 461
[16] Gao X, Du C, Li Y, Song C, Hao Z Q and Lin J Q 2014 *Acta Phys. Sin.* **63** 095203 (in Chinese)
[17] Ghebregziabher I, Hartig K C and Jovanovic I 2016 *Opt. Express* **24** 5263
[18] Zhao S Y and Gao X 2019 *OSA Continuum* **2** 116
[19] Yao S, Zhang J, Gao X, Zhao S Y and Lin J Q 2018 *Opt. Commun.* **425** 152
[20] Hao Z Q, Zhang J, Lu X, Xi T T, Li Y T, Yuan X H, Zheng Z Y, Wang Z H, Ling W J and Wei Z Y 2006 *Opt. Express* **14** 773
[21] Li S Y, Guo F M, Song Y, Chen A M, Yang Y J and Jin M X 2014 *Phys. Rev. A* **89** 023809
[22] Deng Y P, Zhu J B, Ji Z G, Liu J S, Shuai B, Li R X, and Xu Z Z 2006 *Opt. Lett.* **31** 546
[23] Valenzuela A, Munson C, Porwitzky A, Weidman M and Richardson M 2014 *Appl. Phys. B* **116** 485
[24] Harilal S S, Yeak J, Brumfield B E and Phillips M C 2016 *Opt. Express* **24** 17941
[25] Xu W P, Chen A M, Wang Q Y, Zhang D, Wang Y, Li S Y, Jiang Y F and Jin M X 2019 *J. Anal. At. Spectrom.* **34** 1018
[26] Couairon A and Mysyrowicz A 2007 *Phys. Rep.* **441** 47
[27] Xu W P, Chen A M, Wang Q Y, Zhang D, Wang Y, Li S Y, Jiang Y F and Jin M X 2019 *J. Anal. At. Spectrom.* **34** 1018
[28] Wang W, Sun L X, Wang G D, Zhang P and Qi L F 2020 *J. Anal. At. Spectrom.* **35** 357
[29] Maury C, Sirven J B, Courouau J L, Tabarant M and Vercouter T 2013 *Spectrochim. Acta B: At. Spectrosc.* **82** 28
[30] Haddad J E, Canioni L and Bousquet B 2014 *Spectrochim. Acta B: At. Spectrosc.* **101** 171
[31] Guo L B, Zhu Z H, Li J M, Tang Y, Tang S S, Hao Z Q, Li X Y, Lu Y F and Zeng X Y 2018 *Opt. Express* **26** 2634
[32] Li S Y and Jin M X 2016 *China Sci. Paper* **011** 1934 (in Chinese)